Kinetic description of ionospheric outflows based on the exact form of Fokker-Planck collision operator: Electrons

George V. Khazanov,[1] Ildar K. Khabibrakhmanov,[2] and Alex Glocer[1]

[1] We present the results of a finite difference implementation of the kinetic Fokker-Planck model with an exact form of the nonlinear collisional operator. The model is time dependent and three-dimensional; one spatial dimension and two in velocity space. The spatial dimension is aligned with the local magnetic field, and the velocity space is defined by the magnitude of the velocity and the cosine of pitch angle. An important new feature of model, the concept of integration along the particle trajectories, is discussed in detail. Integration along the trajectories combined with the operator time splitting technique results in a solution scheme which accurately accounts for both the fast convection of the particles along the magnetic field lines and relatively slow collisional process. We present several tests of the model's performance and also discuss simulation results of the evolution of the plasma distribution for realistic conditions in Earth's plasmasphere under different scenarios.

1. Introduction

[2] Magnetosphere-ionosphere (MI) coupling has interested scientists for decades, and in spite of experimental and theoretical research efforts, it remains one of the least understood dynamical processes in space plasma. The reason for this is that the numerous physical processes associated with MI coupling occur over multiple spatial and temporal scales. One typical example of MI coupling is the production of upflowing ion events (or ionospheric outflows), such as auroral acceleration, ion energization in the cleft ion fountain, convective heating, polar wind, and plasmaspheric refilling. The classification of ionospheric outflows contributing to MI coupling has frequently been divided into two broad physical categories. The first of these is the polar wind which exists on high-latitude field lines connecting to the interplanetary medium and the geomagnetic tail. Several tutorials by *Schunk* [1986, 1988a, 1988b] and reviews by *Ganguli* [1996] and *Yau et al.* [2007] provide a complete picture of the historical development of polar wind studies. The second region where ionospheric outflows are important is the plasmasphere, where closed field lines allow this region of the inner magnetosphere to become saturated with thermal ions (e.g., see the review by *Singh and Horwitz* [1992]).

[3] The present generation of ion upflow models is based either on a truncated series of higher-order velocity moments [e.g., *Schunk and Watkins*, 1979; *Barakat and Schunk*, 1982a, 1982b; *Mitchell and Palmadesso*, 1983; *Khazanov et al.*, 1984; *Gombosi et al.*, 1985; *Singh and Schunk*, 1985; *Gombosi and Killeen*, 1987; *Ganguli and Mitchell*, 1987; *Ganguli et al.*, 1993; *Rasmussen and Schunk*, 1988; *Demars and Schunk*, 1989, 1994; *Moffett et al.*, 1989; *Singh and Torr*, 1990; *Körösmezey et al.*, 1992] or on kinetic methods including simplified hybrid PIC simulations [e.g., *Barakat and Lemaire*, 1990; *Wilson et al.*, 1990; *Demars and Schunk*, 1989, 1992; *Wilson*, 1992; *Barakat et al.*, 1993, 1995; *Miller et al.*, 1993, 1995; *Barakat and Schunk*, 2001; *Horwitz and Zeng*, 2009; *Barghouthi et al.*, 2011] and direct solution of the kinetic equations [e.g., *Lemaire and Scherer*, 1972; *Lie-Svendsen and Rees*, 1996; *Khazanov et al.*, 1997].

[4] These techniques have been further applied to study the global nature of ion upflow [e.g., *Schunk and Sojka*, 1989; *Gardner and Schunk*, 2004; *Barakat and Schunk*, 2006; *Glocer et al.*, 2009]. Both of these methods have powerful strengths and considerable weaknesses that have been reviewed and discussed by *Echim et al.* [2011].

[5] The higher-order fluid models have serious limitations when they are applied to regions where collisions are infrequent or negligible. These limitations are a result of a fundamental approximation used by all generalized transport models: the models are based on a perturbation approach which assumes distribution functions are close to Maxwellian or bi-Maxwellian. This approximation makes fluid models computationally efficient, but limits their applicability at higher altitudes. The bi-Maxwellian based perturbation approaches are more appropriate for gyration dominated plasma, but still require collisional dominance. It is well known that collisions drive the distribution function toward

[1]NASA Goddard Space Flight Center, Greenbelt, Maryland, USA.
[2]Thomas J. Watson Research Center, IBM, Yorktown Heights, New York, USA.

Corresponding author: A. Glocer, Heliophysics Science Division, NASA Goddard Space Flight Center, Mail Code 673, Greenbelt, MD 20771, USA. (alex.glocer-1@nasa.gov)

equilibrium: this process is the physical reason behind all velocity moment based approximations. A natural consequence of this is that as collisions become less and less frequent, the velocity distribution can develop highly nonequilibrium features (such as conics or double humps) that cannot be accounted for with perturbation methods. To put it plainly, generalized transport methods lose validity in collisionless regimes and must be replaced by a kinetic treatment.

[6] True kinetic methods provide a full solution for the multispecies phase-space distribution function with respect to seven independent variables: time, three-dimensional location, and the particle velocity vector. Results from a kinetic solution can be directly compared with in situ observations of the ion distributions by spectrometers on rockets and satellites with no need to take moments of the measurements. The full informational content of the data may be exploited in this type of comparison. By looking for characteristic "signatures" in the distribution function, one would be able to identify which physical mechanisms are responsible for certain ion outflow events.

[7] The disadvantage of a kinetic treatment is that it is computationally demanding, and that development of adequate solution methods is not straightforward. Presently no existing plasma outflow model is based on such an approach and it is not likely that anyone will be able to develop one in the near future. Also, most of the previous kinetic ionospheric outflow studies have used the statistically based Monte Carlo technique [e.g., *Barakat and Lemaire*, 1990; *Wilson*, 1992; *Miller et al.*, 1993; *Barghouthi et al.*, 1993]. This method is encumbered with random uncertainties from the particle simulation, as described by *Miller and Combi* [1994] and *Barakat et al.* [1998]. Therefore, great care must be taken when applying this technique.

[8] Another approach, and the one applied in this study, is to use the Fokker-Planck collisional operator, similar to the studies by *Khazanov et al.* [1994] and *Lie-Svendsen and Rees* [1996]. The main development of this paper and the difference from all previous studies, however, is the use of the exact form of the Fokker-Planck collisional operator without any assumptions with respect to the distribution function of the background particles. In this study the nonlinear form of the Fokker-Planck collisional operator has been solved self-consistently for the first time for space plasma applications. This method will not have to deal with the statistical uncertainties of a particle simulation because the solution procedure of such a problem is not statistical in nature [see *Khazanov et al.*, 1994; *Khazanov and Liemohn*, 1995]. For the sake of simplicity, this paper will only focus on the electron distribution function formation, leaving the discussion of electrodynamic and Coulomb electron-ion coupling to our forthcoming paper. It should be noted though that the numerical approach developed here will be exactly the same for the ion population of space plasma and is therefore presented here in rather general form.

2. The Fokker-Planck Kinetic Equation

[9] As mentioned above, we will use the exact form of the Fokker-Planck collisional operator to develop a complete kinetic description of ionospheric plasma outflows from the collision-dominated region to the collisionless magnetospheric plasma. Such an approach provides a continuous calculation of

the self-consistent coupling processes between the different components of the ionospheric and magnetospheric plasmas along geomagnetic field lines. The Fokker-Planck kinetic equation, written in terms of the two Rosenbluth potentials $H_\alpha(\mathbf{v})$ and $G_\alpha(\mathbf{v})$, in the presence of gravitational $\mathbf{g}$, electric $\mathbf{E}$ and magnetic $\mathbf{B}$ fields can be presented in the following general form [*Rosenbluth et al.*, 1957; *Shkarofsky et al.*, 1966]:

$$\frac{\partial f}{\partial t} + \mathbf{v} \cdot \nabla_r f + \left[\mathbf{g} + \frac{e}{m} \left(\mathbf{E} + \frac{1}{c} \mathbf{v} \times \mathbf{B} \right) \right] \cdot \nabla_v f = \sum_\alpha \frac{4\pi n_\alpha n e^2 e_\alpha^2}{m_\alpha m}$$
$$\cdot \ln \Lambda \left[-\frac{\partial}{\partial v_i} \left(f \frac{\partial H_\alpha}{\partial v_i} \right) + \left[\frac{1}{2} \frac{\partial^2}{\partial v_i \partial v_j} \left(f \frac{\partial^2 G_\alpha}{\partial v_i \partial v_j} \right) \right] \right] \quad (1)$$

Here $f = f(t, \mathbf{r}, \mathbf{v})$ is the distribution function, where $\mathbf{r}$ and $\mathbf{v}$ are the position and velocity vectors, respectively; index α denotes the background species with which the particle with charge e and mass m collides; and n_α is the density of the species α. The Rosenbluth potentials $H_\alpha(\mathbf{v})$ and $G_\alpha(\mathbf{v})$ are integrals over the distribution of the background particles

$$H_\alpha(\mathbf{v}) = \frac{m + m_\alpha}{m_\alpha} \int \frac{f_\alpha(\mathbf{v}')}{|\mathbf{v} - \mathbf{v}'|} d^3\mathbf{v}'$$
$$G_\alpha(\mathbf{v}) = \frac{m + m_\alpha}{m_\alpha} \int f_\alpha(\mathbf{v}') |\mathbf{v} - \mathbf{v}'| d^3\mathbf{v}' \quad (2)$$

[10] Previous use of the Fokker-Planck collisional operator for ionospheric plasma outflows was restricted to its simplified, linearized, form by assuming that the thermal background electrons and ions are static and have Maxwellian distribution functions. This greatly simplifies the calculation of the Rosenbluth potentials and equation (2) can be presented in an analytical form. Such a linearized Coulomb collisional operator has been used in earlier calculations of superthermal electron transport [*Khazanov et al.*, 1979; *Yasseen et al.*, 1989; *Khazanov et al.*, 1994] and in the polar wind model by *Lie-Svendsen and Rees* [1996]. It should be stressed, however, that in some cases the departure of the plasma distribution function from a Maxwellian or bi-Maxwellian can be very large, causing the linearized Fokker-Planck collisional operator to lose validity. For example, [*Barakat et al.*, 1995], using their Monte Carlo model, found that between the low-altitude collision-dominated and high-altitude collisionless regions, the H^+ velocity distribution becomes double-humped in energy. The formation of this double hump is a natural consequence of the interplay between the electrostatic ion acceleration and the velocity-dependent Coulomb (H^+–O^+) collisions. It may also occur in other regions of space plasma and should be rigorously analyzed with the model being proposed in this study. This will be the case not only for the ions but also for the electrons. Such a unified treatment for the electron distribution function is especially needed in the presence of superthermal electrons. Artificial separation of the electron distribution function into thermal and superthermal parts leads, in some cases, to unrealistically high values of electron temperatures and particle fluxes [*Tam et al.*, 1995].

[11] As we pointed out in section 1, we use the exact form of the Coulomb collisional operator (1) without any assumptions with respect to the distribution function of the background particles. In this case, the collisional operator becomes nonlinear and depends on the plasma distribution
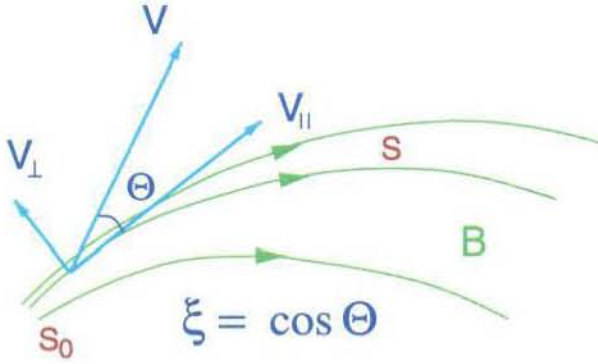
Figure 1. Geometry of the problem. Spatial coordinate s along the magnetic field line. Principal variables in velocity space are the velocity of the particle v and cosine of pitch angle $\xi = \cos\theta$.

function itself because collisions between similar particles may no longer be neglected. Also, we expect that in some cases the departure of the plasma distribution function from Maxwellian can be very large and the linearized Fokker-Planck collisional operator can lose validity, even for the interaction between different kinds of particles. To deal with this problem, we will transform equation (1) into a computationally manageable form below, as established and described by *Khazanov et al.* [1979, 1994, 1996; *Khazanov and Liemohn*, 1995] for the case of superthermal electron transport. Nonlinearity in equation (1) will be handled using an iterative scheme similar to the case when we used the isotropic part of the Fokker-Planck collisional operator to calculate the electron distribution function in the collision-dominated region [*Khazanov et al.*, 1978, 1979].

[12] Another type of nonlinearity occurs in our model through the development of the self-consistent electric field that is part of the calculation of the hydrodynamic model and the Fokker-Planck kinetic equation (1). The reason for the formation of a self-consistent potential in a collisionless plasma is this: high mobility electrons tend to overtake ions. As a result, the electric neutrality of the plasma is violated and an electric field appears which constrains the electrons, forcing them, on average, to travel together with the ions. This field also significantly affects the motion of the ions by accelerating them. The electric field acts as a catalyst by transferring the pressure of the electron gas to the plasma ions; this pressure is proportional to the electron temperature, T_e. Therefore, when $T_e \approx T_i$, the effects of the self-consistent electric field and the effects of the ions' thermal motion are generally of the same order of magnitude. Photoelectrons, which form due to ionization of the atmosphere by solar radiation, can alter the self-consistent potential in the space plasma. The presence of the enhanced high-velocity tail in the electron distribution will increase the number of fast ions. Due to the enhanced ion acceleration in an expanding plasma, the initial superthermal electron distribution function could be changed. As we pointed out in the Introduction, the electrodynamic electron-ion coupling will be ignored in our current study for sake of simplicity. The calculation of the self-consistent electric field will be included in the iteration loop of the model in future studies, similar to the descriptions

of *Khazanov et al.* [1997], based on the quasi-neutrality and currentless conditions.

3. Description of the Model

[13] In the Earth's strong magnetic field the distribution function is highly symmetric in the plane transverse to the magnetic field direction. It is therefore convenient to choose the spatial coordinate 's' along the local magnetic field line and in the velocity space to choose the spherical system of coordinates with polar axis along the local magnetic field line (Figure 1).

[14] Under assumption of azimuthal symmetry of the distribution function the equation (1) is transformed to the form

$$\frac{\partial f}{\partial t} + \xi v \frac{\partial f}{\partial s} - \frac{1-\xi^2}{2} v \frac{1}{B} \frac{\partial B}{\partial s} \frac{\partial f}{\partial \xi} = \hat{L}(f) \tag{3}$$

Here we omitted gravitational and electric fields. The variable ξ, is the cosine of the angle between particle velocity vector and magnetic field direction, or in other words it is cosine of the pitch angle, which in our geometry corresponds to the polar angle. Only inhomogeneity of the magnetic field is included in the last term of the left hand side. This term is responsible for conservation of the adiabatic moment of the particle in the absence of collisions

$$\frac{1-\xi^2}{B} = \frac{1-\xi_0^2}{B_0} = \text{const} \tag{4}$$

and represents the most important dynamic effect of trapping particles in the Earth's magnetic field.

[15] The Coulomb collisional operator will be in its exact form, similar to [*Khabibrakhmanov and Khazanov*, 2000], which in spherical system of reference in velocity space takes the following form:

$$\frac{1}{\Gamma}\hat{L}(f) = \frac{1}{v^2}\frac{\partial}{\partial v}v^2\left[D_{vv}\frac{\partial f}{\partial v} + D_v f + D_{v\xi}\frac{\partial f}{\partial \xi}\right]$$
$$+ \frac{\partial}{\partial \xi}\left[D_{\xi\xi}\frac{\partial f}{\partial \xi} + D_\xi f + D_{\xi v}\frac{\partial f}{\partial v}\right] \tag{5}$$

Here, collisional strength is defined by

$$\Gamma_\alpha = \frac{4\pi e^4 \ln\Lambda}{m^2} \tag{6}$$

and Fokker-Planck coefficients can be expressed as

$$D_{vv} = \frac{1}{2}\frac{\partial^2 G}{\partial v^2} \tag{7}$$

$$D_v = \frac{1}{2}\frac{\partial}{\partial v}\left[\frac{1}{v^2}\frac{\partial}{\partial v}v^2\frac{\partial G}{\partial v} + \frac{1}{v^2}\frac{\partial}{\partial \xi}(1-\xi^2)\frac{\partial G}{\partial \xi} - 2H\right] \tag{8}$$

$$D_{\xi v} = D_{v\xi} = \frac{1-\xi^2}{2v}\frac{\partial^2}{\partial \xi \partial v}\frac{G}{v} \tag{9}$$

$$D_{\xi\xi} = \frac{1-\xi^2}{2v^2}\left[\frac{1-\xi^2}{v^2}\frac{\partial^2 G}{\partial \xi^2} + \frac{1}{v}\frac{\partial G}{\partial v} - \frac{\xi}{v^2}\frac{\partial G}{\partial \xi}\right] \tag{10}$$

$$D_\xi = \frac{1-\xi^2}{2v^2}\frac{\partial}{\partial \xi}\left[\frac{1}{v^2}\frac{\partial}{\partial v}v^2\frac{\partial G}{\partial v} + \frac{1}{v^2}\frac{\partial}{\partial \xi}(1-\xi^2)\frac{\partial G}{\partial \xi} - 2H\right] \tag{11}$$

in terms of the Rosenbluth potentials G and H. The integral definitions (equation (2)) for these potentials are equivalent to couple of Poisson equations in the velocity space

$$\Delta_v H = -f, \quad \Delta_v G = H \tag{12}$$

As was originally suggested by *Rosenbluth et al.* [1957], it is convenient to use a truncated series of Legendre polynomials $L_k(\xi)$ for the expansion in the angle variable ξ

$$f(v, \xi) = \sum_{k=0}^{N} f_k(v) L_k(\xi) \tag{13}$$

This type of expansion has been widely used in fusion research [e.g., *Killeen et al.*, 1976], where magnetic particle trapping and collisional transport is very sensitive to fine details of the plasma particle distribution function. *Khazanov* [1979] also used this approach in order to describe ionosphere-plasmasphere transport of superthermal electrons. *Pierrard and Lemaire* [1998] as well as *Pierrard et al.* [2001] used similar expansions to study the polar wind and, more recently, to obtain a self-consistent description of the electrons in the solar wind.

[16] For the expansion coefficients $H_k(v)$ and $G_k(v)$ then we have a set of second-order ordinary differential equations:

$$\frac{\partial}{\partial v} v^2 \frac{\partial}{\partial v} H_k - k(k-1) H_k = -v^2 f_k \tag{14}$$

$$\frac{\partial}{\partial v} v^2 \frac{\partial}{\partial v} G_k - k(k-1) G_k = v^2 H_k \tag{15}$$

with appropriate boundary conditions. The solution again can be expressed in terms of corresponding Green's function [*Rosenbluth et al.*, 1957], for numerical purposes; however, it is more convenient to solve corresponding boundary value problems using standard finite difference approximation.

[17] It is convenient at this point to transform to dimensionless variables. The spatial variable is normalized to the length of the given magnetic field line S so that dimensionless length along the field line varies from -1 to 1 when particle moves from the boundary in Northern Hemisphere to the conjugate point in the Southern Hemisphere

$$s \rightarrow -1 + 2s/S$$

We fix the maximum value of the velocity of the particle on the grid V. With this choice the characteristic timescale of the problem becomes S/V, which is the time required for fastest particles under consideration to travel the distance S. In dimensionless variables equation (3) still has the same form with dimensionless collisional strength defined as

$$\Gamma = \frac{4\pi e^4 S n \ln \Lambda}{m^2 V^4} \tag{16}$$

Here we also assumed that distribution function is normalized to unity. Therefore, the problem is characterized by only one dimensionless parameter, the relative strength of the collisional operator. This is very important step. As a result, every numerical solution presented in the paper represents a whole family of solutions. Changes in physical plasma

density n and scaling velocity V such that n/V^4 leaves the parameter Γ unchanged do not affect the solution of the problem. Of course the interpretation of the result will change as the "kinematic" timescale is still defined by $\tau = S/V$ and the physically most meaningful interpretation of the dimensionless parameter Γ is the ratio of that "kinematic" timescale to collisional timescale. When $\Gamma \ll 1$ is small we expect most of the particles collide very rarely with distribution function deviating strongly from Maxwellian. In opposite regime $\Gamma \gg 1$ the distribution function is expected to stay close to Maxwellian form and the details of the deviation of the distribution function are fully described by the value of the parameter and physical nature of the operator in the right hand site. The results are also invariant under change of the particles mass and charge which conserve the factor Γ.

[18] Equation (3) is subject to boundary conditions. In the spatial variable we specify the distribution function at $s = -1$ and $s = 1$. In the velocity space it is required that the flux of the particles across the boundaries vanish. For the angular variable corresponding fluxes vanish automatically as the Fokker-Planck coefficients $D_{\xi\xi}, D_\xi, D_{\xi v}$ are equal zero there. In velocity variable some of the Fokker-Planck coefficients are singular at $v = 0$, for instance $D_{\xi\xi}$, and the boundary condition

$$\left. \frac{\partial f}{\partial v} \right|_{v=0} = 0$$

must be imposed. In the past, *Khazanov* [1979] and *Pierrard and Lemaire* [1998] used this "regularity condition" to avoid singularities which appear at $v = 0$.

4. Numerical Implementation

[19] Numerical implementation of the equation (3) follows the general scheme of time splitting for multidimensional problems [*Marchuk*, 1975].
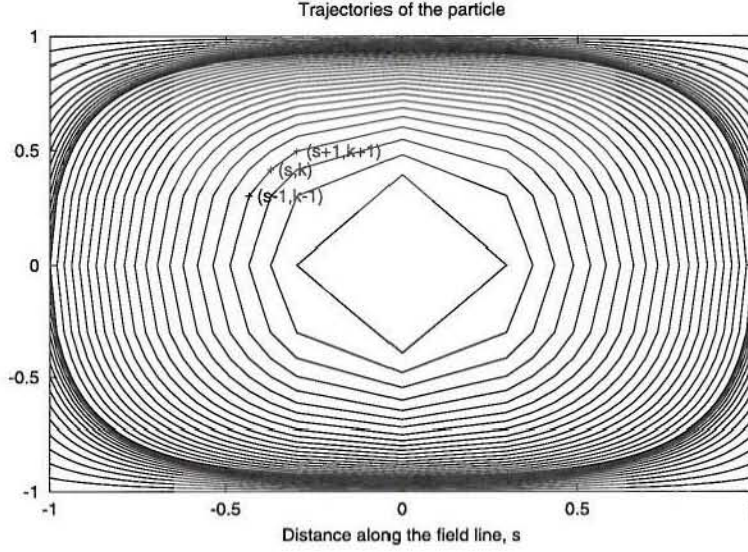
4.1. Integration Along the Trajectories

[20] In the absence of collisions the left hand side of equation (3) conserves the adiabatic moment of the particle given by (4). Therefore, for a given magnetic field profile $B(s)$ the particle moves in the plane $(s; \xi)$ along the trajectories defined by the integral of motion (4). These trajectories are independent of particle velocity v and are shown in Figure 2 for dipole magnetic field as the lines connecting the grid points. If we choose particular grid point $(s; k)$ in this plane as shown in Figure 2, the points $(s+1; k+1)$ and $(s-1; k-1)$ belong to the same trajectory. We can expand the value of the distribution function $f_{s+1; k+1}$ at the point $(s+1; k+1)$ in Taylor series

$$f_{s+1,k+1} = f_{s-1,k-1} + \left(\frac{\partial f}{\partial s}\right)_{s,k} (s_{s+1} - s_{s-1})$$
$$+ \left(\frac{\partial f}{\partial \xi}\right)_{s,k} (\xi_{k+1} - \xi_{k-1}) + \dots \tag{17}$$

From expression (17) the centered spatial derivative in the (s, ξ) plane at the grid point $(s; k)$ is approximated as

$$\xi \left(\frac{\partial f}{\partial s}\right)_{s,k} = \frac{f_{s+1,k+1} - f_{s-1,k-1}}{z_{s+1} - z_{s-1}} - \left(\frac{\partial f}{\partial \xi}\right)_{s,k} \frac{\xi_{k+1} - \xi_{k-1}}{z_{s+1} - z_{s-1}} \tag{18}$$

Figure 2. Trajectories of the particles in (s, ξ) plane as defined by the conservation of the magnetic moment of the particle.

here we also took into account that $\xi = \xi(s)$ along the trajectory and used new variable z

$$z = \int \frac{ds}{\xi(s)}.$$

Using approximation (18) in the left hand side of (3)

$$\left(\frac{\partial f}{\partial t}\right)_{s,k} + v\left[\frac{f_{s+1,k+1} - f_{s-1,k-1}}{z_{s+1} - z_{s-1}} - \left(\frac{\partial f}{\partial \xi}\right)_{s,k}\frac{\xi_{k+1} - \xi_{k-1}}{z_{s+1} - z_{s-1}}\right. $$
$$\left. - \left(\frac{1 - \xi^2}{2}\frac{1}{B}\frac{dB}{ds}\frac{\partial f}{\partial \xi}\right)_{s,k}\right] \tag{19}$$

one can see that the last two terms cancel each other when

$$\frac{\xi_{k+1} - \xi_{k-1}}{z_{s+1} - z_{s-1}} = -\left(\frac{1 - \xi^2}{2}\frac{1}{B}\frac{dB}{ds}\right)_{s,k} \tag{20}$$

But this is just a finite difference approximation of the equation for trajectories (4). In other words, when grid points $(s - 1, k - 1)$ and $(s + 1, k + 1)$ belong to the same trajectory as point (s, k), the left-hand side of equation (3) has simple finite difference approximation

$$\left(\frac{\partial f}{\partial t}\right)_{s,k} + v\frac{f_{s+1,k+1} - f_{s-1,k-1}}{z_{s+1} - z_{s-1}} \tag{21}$$

and conservation of the adiabatic moment of the particle is accounted by nonuniform grid, where all the grid points belong to trajectories of the particle. As we show section 4.2, this procedure is able to completely eliminate numerical diffusion in the absence of collisions. We note that *Lie-Svendsen and Rees* [1996] also obtained a solution to the Fokker-Planck equation for the case of polar wind minor ion outflow, but they used a standard finite difference rather than our approach which chooses grid points belonging to the

trajectories of the particles in absence of collisions. Moreover, their approach was for a steady state solution, while our approach is for a time-dependent solution.

4.2. Time Splitting

[21] The time splitting technique allows one to use independent approximations of the differential operators acting in each of the independent variables. Equation (3) is represented as

$$\frac{\partial f}{\partial t} = \sum_{i=1}^{M} \hat{L}_i f \tag{22}$$

Then M equations

$$\frac{\partial f_i}{\partial t} = \hat{L}_i f, \quad i = 1...M \tag{23}$$

are solved in succession using as an initial value result of the previous fractional time step f_{i-1}. This technique is very flexible in allowing addition of new terms. The second-order approximation in time can be achieved by proper choice of the operator splitting in representation (22).

4.3. Testing the Code

[22] In this section we will validate the quality of the numerical approach. In particular, we will carry out four carefully crafted tests that demonstrate the model's fidelity to the well known properties of the Coulomb collisional operator, the model's low numerical diffusion, and a comparison with previous models. The following list provides a short description of each test with the complete results and details left to sections 4.3.1–4.3.4.

[23] 1. One of the most important properties of the Coulomb operator is conservation of density and energy of the distribution during the process of relaxation toward a Maxwellian form. We test the Coulomb collision operator with a

t=1.0   t=4.0

t=8.0   t=11.0
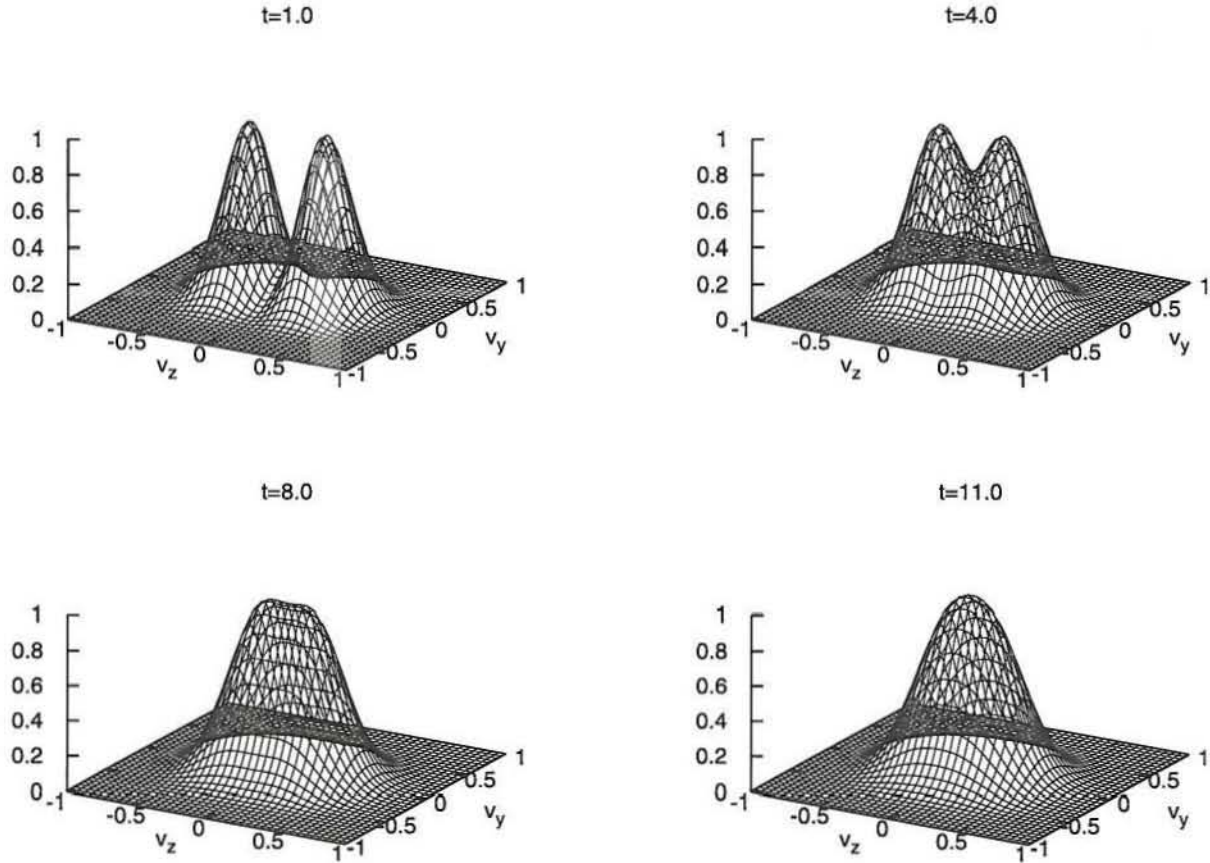
Figure 3. Relaxation of the initial streaming distribution function (24) toward Maxwellian.

fairly arbitrary initial distribution and follow its relaxation to a Maxwellian distribution (section 4.3.1).

[24] 2. An important property of the transport operator in the left hand side of equation (3) is the complete isolation of the trapping region from the loss cone. In the absence of the collisions, particles are trapped in the equatorial region or are freely moving along a magnetic field line from one end to the other; there is no diffusion into or out of the trapped region. We test this property by turning off the collision terms and considering an upflowing population in the ionosphere that completely fills the loss cone region (section 4.3.2).

[25] 3. Inside the trapped region any initial nonuniformity of the distribution function along the trajectory of the particle becomes quickly "bounce" averaged and uniform. We illustrate that important property by considering convective phase mixing of the distribution in the absence of collisions (section 4.3.3).

[26] 4. Sharp boundaries can appear between trapped and free motion regions as result of collisions. This effect was the subject of numerous studies in the past. We compare our model results against these previous studies as an additional test (section 4.3.4).

4.3.1. Relaxation to Maxwellian Distribution

[27] In this test the convection term was turned off. It is assumed that distribution function is independent of the spatial variable but has an arbitrary dependence on velocity and pitch angle. Figure 3 consists of several snapshots of the time evolution of an initial distribution defined by

$$F(\xi, v) = 10v^2 \exp(-v^2/0.08)\xi^2 \qquad (24)$$

The space–pitch angle grid corresponds to $L = 2$ with total of 75 grid points at the equator. The number of velocity grid points has been taken to be 64. Although the problem has been solved in spherical system of coordinates in velocity space, the results have been transformed to $v_\perp = v\cos\theta$, $v_\parallel = v\sin\theta$ space for presentation. In this test, special attention has been drawn to the conservation properties of the numerical model. It was found that density and energy of the distribution is conserved within a fraction of a percent on collisional time scales (Figure 3).

[28] The final distribution is shown in Figure 4. Here the difference between calculated distribution function and Maxwellian $0.9 \exp(-v^2 / 0.08)$ has been plotted for every value of the pitch angle. As we can see, the distribution function has relaxed to a Maxwellian with relative error of a fraction of a percent for all pitch angles.

4.3.2. Loss Cone Passing With No Collisions

[29] The second new feature of the model is integration along the trajectories. This technique helps to virtually
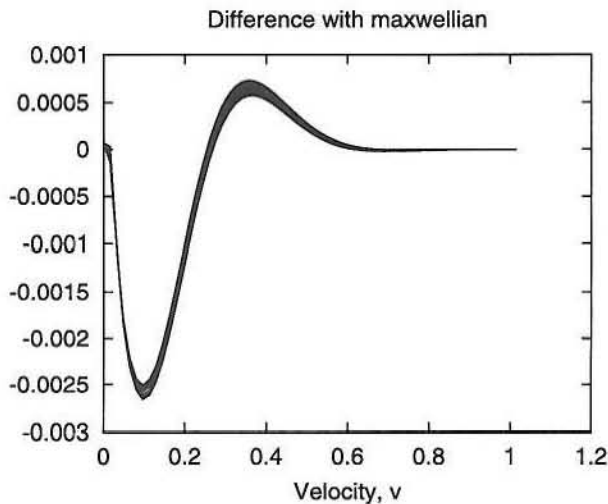
Figure 4. Relaxation of the initial distribution function: approximation error.

eliminate the numerical diffusion across the trajectories in the absence of interparticle collisions. This important property is illustrated in Figure 5. Here the collisions have been turned off, and we start the calculations with an empty magnetic field line. At one of the ionospheric boundary the distribution function is specified such that the loss cone is populated but not the trapped region. As is clear from the results, the trapped region remains completely empty everywhere along the field line with a step-like increase at the loss cone boundary.

4.3.3. Convective Phase Mixing of the Distribution in the Absence of Collisions

[30] As the second test of the concept of integration along particle trajectories the evolution of the initial distribution function with the maxima inside the trapped region has been modeled. Figure 6 (top left) shows an initial distribution which is localized at equator inside the trapped region and is

moving toward the right boundary. The distribution is convected toward the right boundary as can be seen in Figure 6 (top right). Later on, particles are reflected and move back toward the left boundary, as Figure 6 (bottom left). The circulation along the trajectories inside the trapped region is differential. Particles with larger velocity move faster along the trajectories and the initially localized maxima, even for the particles with the same velocity v as in Figure 4, is being dispersed by the differential circulation. At later times (Figure 6, bottom right), the distribution attains a characteristic "hat-like" shape, where distribution is completely smoothed along the particle trajectory. As before, in the absence of collisions there is virtually no diffusion of the particles across the boundary of the trapped region.

[31] The effect of rapid phase mixing of the particles inside the trapped region is the basis for the so-called "bounce-averaged" description of the plasma, where the assumption that the distribution function is constant along the trajectory of the particle in s space considerably simplifies the description.

4.3.4. Comparison With Earlier Model

[32] *Khazanov et al.* [1993] used the linearized coulomb collisional operator in order to study the evolution of superthermal electron component. In their model the mirroring term in equation (3) has been eliminated by direct change of angle variable ξ to ξ_0 according to the adiabatic invariant (4).

[33] In order to verify the concept of integration along the trajectories the test calculation was performed on exactly same, linearized model of *Khazanov et al.* [1993, equation (1)] but using algorithm presented in this paper. The result of the comparison is shown in Figure 7 as an equatorial distribution function for high-energy 50 eV electrons against the pitch angle at the L shell $L = 3$. As shown in Figure 7, integration along the particle trajectories yields a result very close to distribution obtained earlier by a different technique.

5. Results and Discussions

[34] The above tests of the numerical model has demonstrated that it is capable of accounting for particle convection
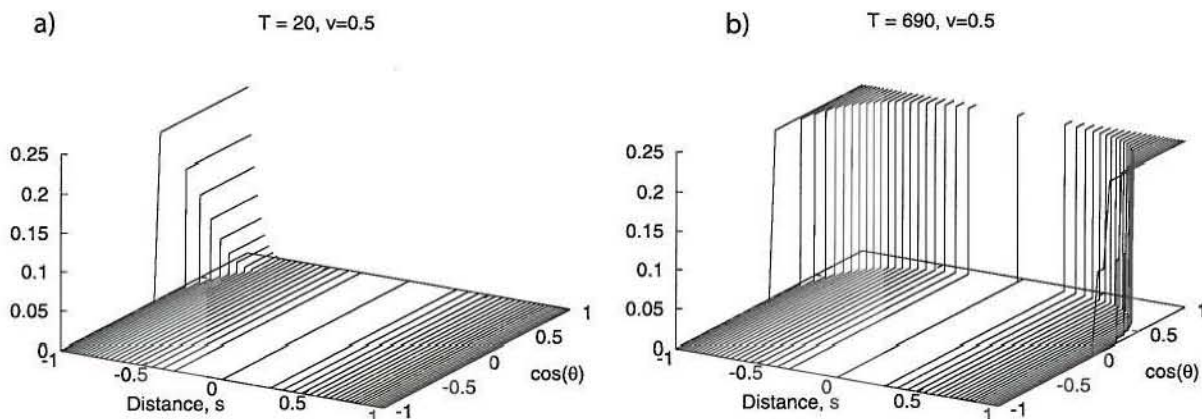
Figure 5. Refilling of the empty field line tube in the absence of collisions. There is no numerical diffusion into the trapped region.
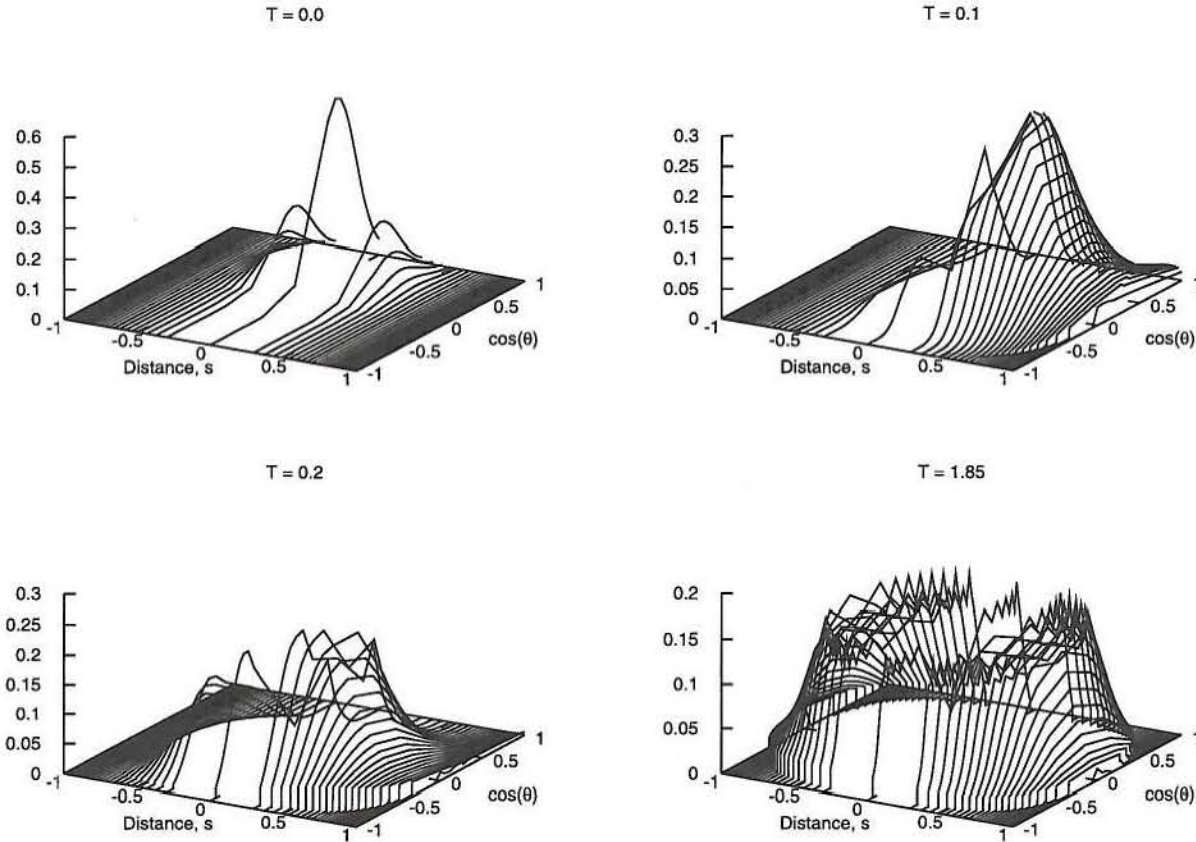
T = 0.0

T = 0.1

T = 0.2

T = 1.85

Figure 6. Phase mixing of the initial distribution function with maximum at the equator.

without introducing spurious numerical diffusion between the loss cone and trapped region. In this section we present results of several simulations of the dynamics of the particle distribution function in the plasmasphere. We assume a magnetic dipole configuration and $L = 2$. In general, however, this model can be adjusted to use an arbitrary magnetic field configuration.

5.1. One-Sided Refilling of the Initially Empty Plasmasphere

[35] As the plasma particles are treated in our model in a self-consistent and unified fashion it is now possible to compute the refilling of completely empty plasmasphere with a given source at the ionospheric boundary. The models with linearized version of collisional operator always assume the presence of a background plasma and therefore are not capable of modeling a completely empty plasmasphere. Moreover, such models are incapable of handling the refilling of the core low-energy plasma.

[36] For $L = 2$ and an initially empty magnetic flux tube, the distribution function at the ionospheric boundary is taken in the form

$$0.1 \exp\left(-v^2/0.05\right) \tag{25}$$

There is no specification of the particles in our model, which is described by only one dimensionless parameter (16). Thus, as we mentioned above, the developed approach is applicable for electron and ions. In Figures 8 and 9 the time evolution of one-sided refilling for parameter value $\Gamma = 1$
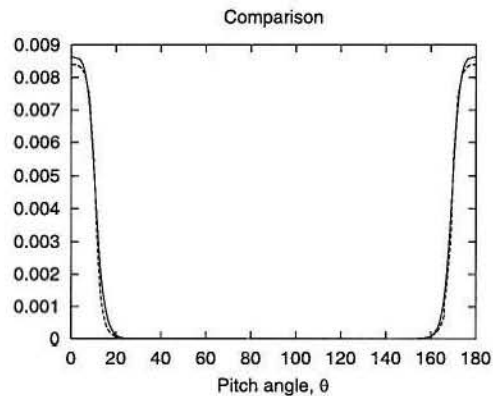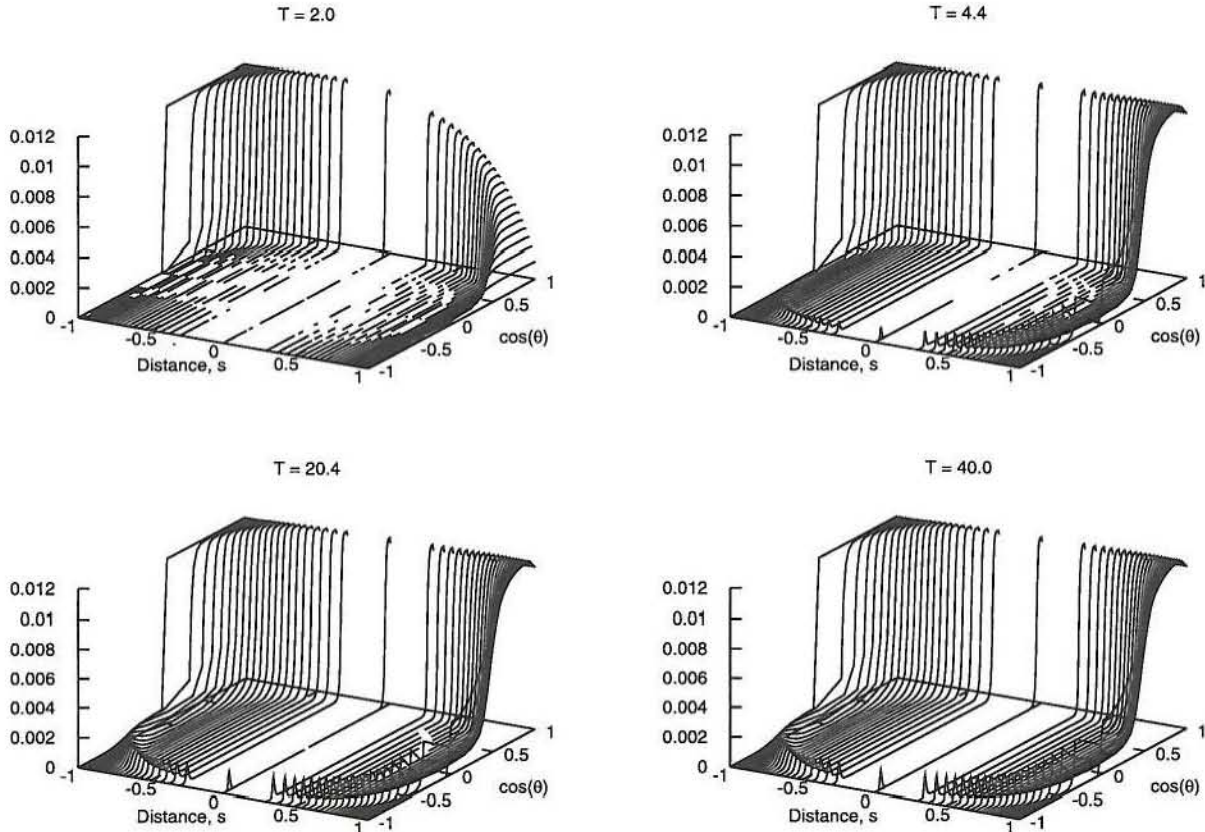
Figure 7. Comparison of the stationary distribution function for 50 eV electrons at the equator $L = 3$ with that computed by *Khazanov et al.* [1993].

Figure 8. One-sided refilling of the empty plasmaspheric tube with $L = 2$: distribution function at $v = 0.5$ as function of the distance s along the field line and cosine of the pitch angle ξ.

is presented. Figure 8 (top left) shows the earlier stage of the refilling process. The loss cone is quickly filled by the source at the left boundary, while the trapped region remains essentially empty. At later times the small amount of slow particles, which has entered trapped region due to finite collisional strength, appears as a component moving backward, from the right to the left (negative ξ). Particles accumulate in the trapped region, with the peak intensity at the boundary of the trapped region.

[37] Finally, a quasi-stationary state is approached, where the detailed balance between convection and collisional diffusion in velocity space gives rise to the distribution function, which is far from a Maxwellian distribution. This is even more clear from the high energy part of the distribution function shown in Figure 10.
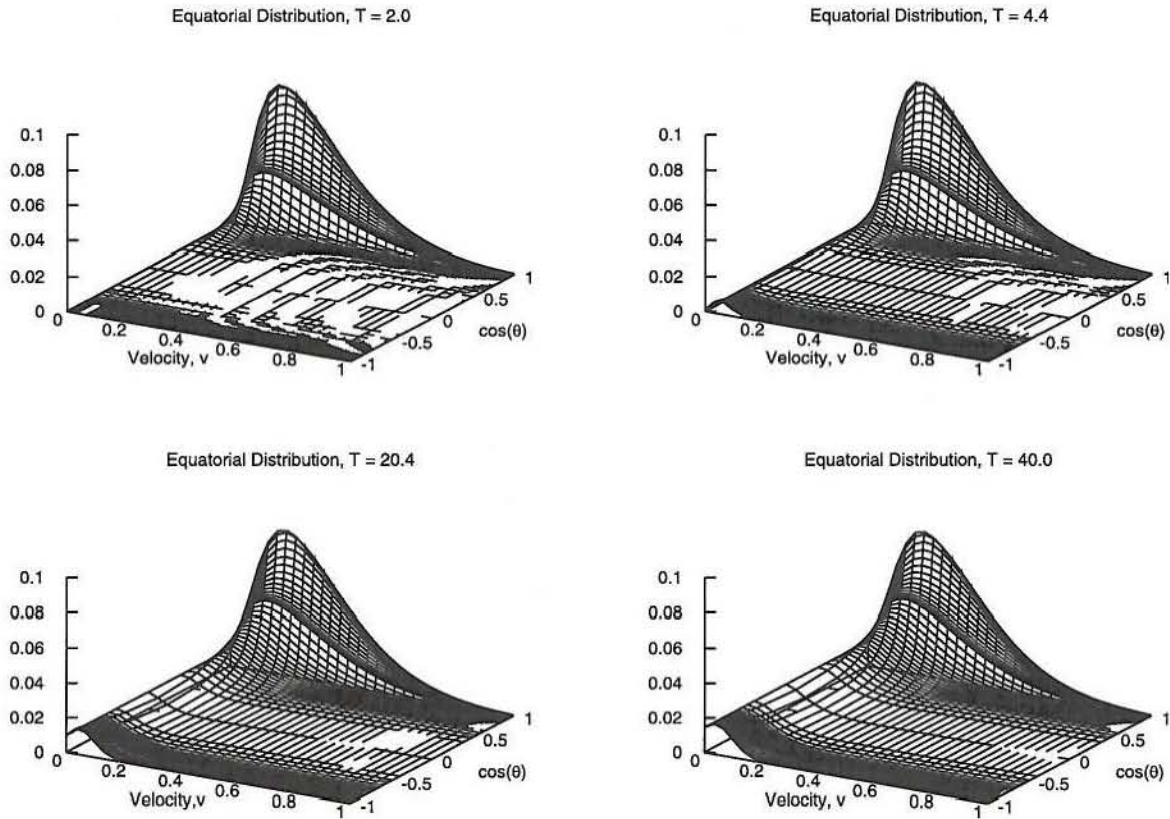
5.2. Relaxation of an Initially Maxwellian Distribution in the Plasmasphere

[38] In order to understand the importance of convection and particle trapping, the model with an initial isotropic Maxwellian distribution has been calculated. The distribution at the boundary and initial distribution throughout the magnetic tube line is Maxwellian. The density of the initial distribution is nonuniform along the field line and is proportional to magnetic field strength $B(s)$. Evolution of the distribution is shown in the same format as before. Figure 11

shows the distribution of particles with $v = 0.67$ for four different times. The distribution near the right boundary of the magnetic tube line, $s = -0.96$ is shown in Figure 12. The redistribution of the particles during the relaxation is clear with a transient appearance of anisotropy and overall change in shape. Although the distribution for long time evolution appears to be isotropic at low and intermediate energies, the strong anisotropy builds at high energies. This is shown in Figure 13 where the high-energy part of the same distribution function as is shown in Figure 11 (bottom right).

5.3. Particle Precipitation Into the Loss Cone With an Initially Maxwellian Distribution Function of Particles

[39] The process of particle precipitation from the plasmaspheric tube is modeled again with an initially isotropic Maxwellian distribution everywhere in the tube. The evolution of the computed distribution function at velocity $v = 0.67$ is shown in Figure 14. The particles quickly precipitate from the loss cone. It takes much longer for particles in the trapped region as a result of collisions to scatter to loss cone and precipitate. The velocity distribution function close to the right boundary at $s = -0.96$ is shown in Figure 15. It is clear that a strongly anisotropic distribution is formed due to the precipitation near the ionospheric boundary. The high-energy tail of the distribution at $T = 800$ is shown separately in Figure 16 and demonstrates that the anisotropy of the

Equatorial Distribution, T = 2.0

Equatorial Distribution, T = 4.4

Equatorial Distribution, T = 20.4

Equatorial Distribution, T = 40.0

Figure 9. One-sided refilling of the empty plasmaspheric tube with $L = 2$: distribution function at $s = -0.96$ as function of the velocity v and cosine of the pitch angle ξ.

Equatorial Distribution, T = 40.0
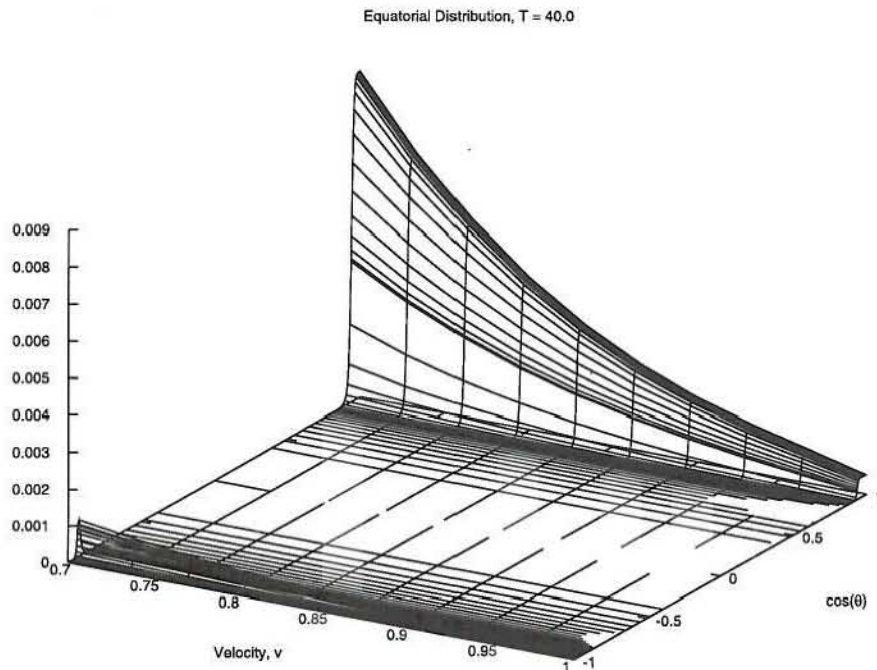
Figure 10. One-sided refilling of the empty plasmaspheric tube with $L = 2$: high-energy part of the distribution function at $s = -0.96$ as function of the velocity v and cosine of the pitch angle ξ.
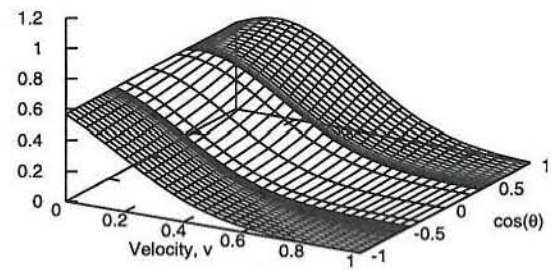
T = 4.0

T = 124

T = 244

T = 400
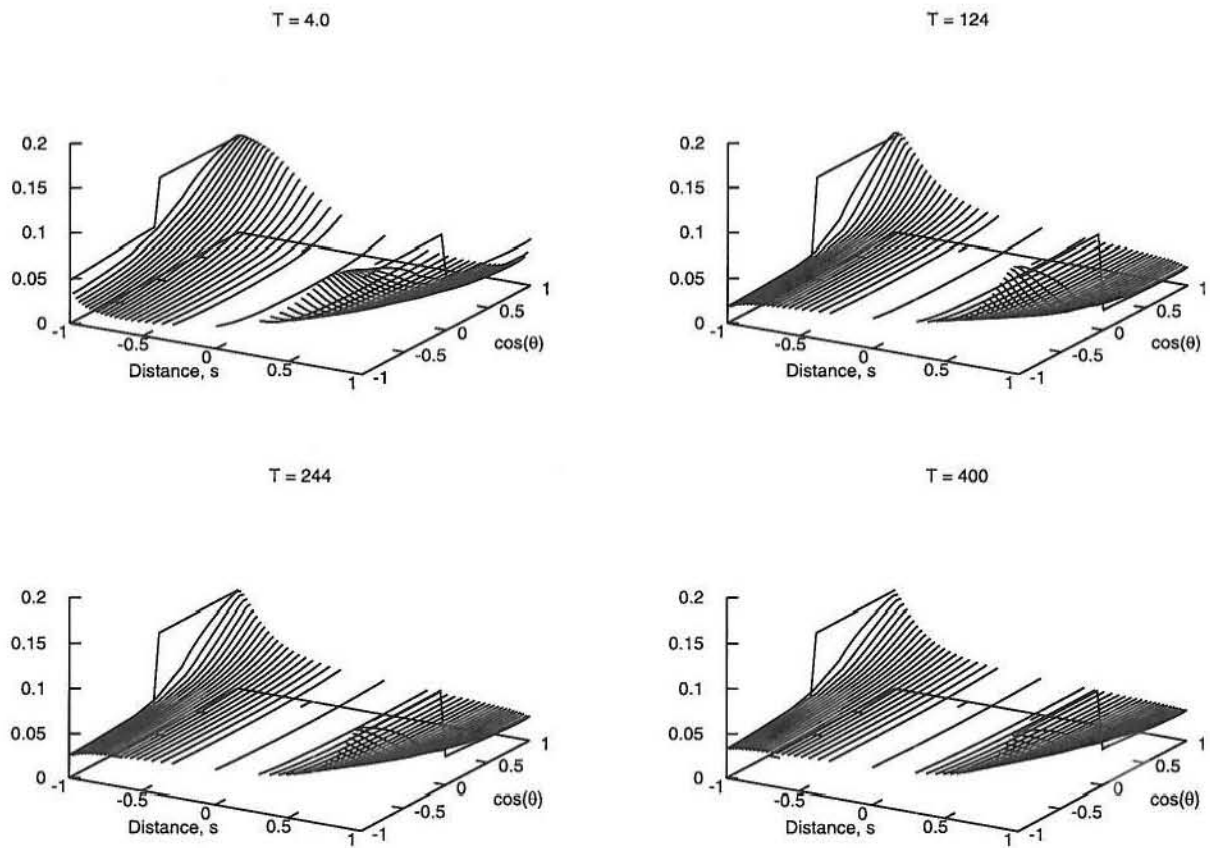
Figure 11. Relaxation of the initial Maxwellian distribution function to stationary distribution at $v = 0.67$ as a function of distance s and the cosine of the pitch angle $\xi = \cos \theta$.
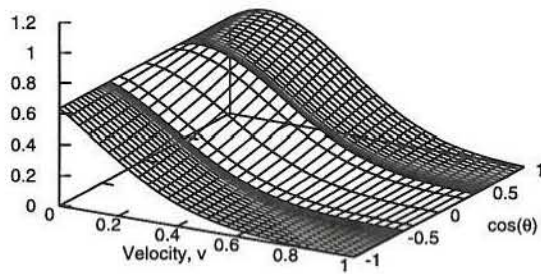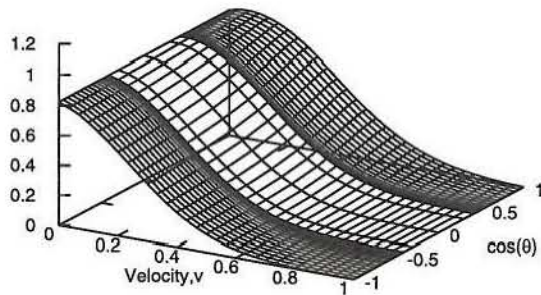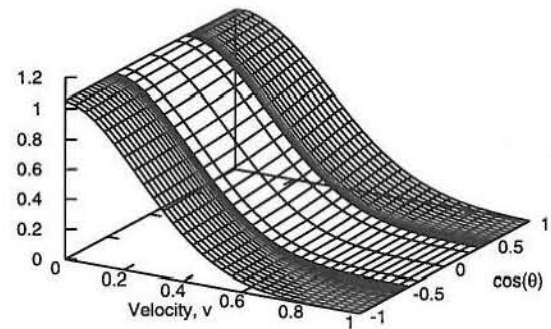
Distribution at s=-0.96, T = 4.0   Distribution at s=-0.96, T = 124

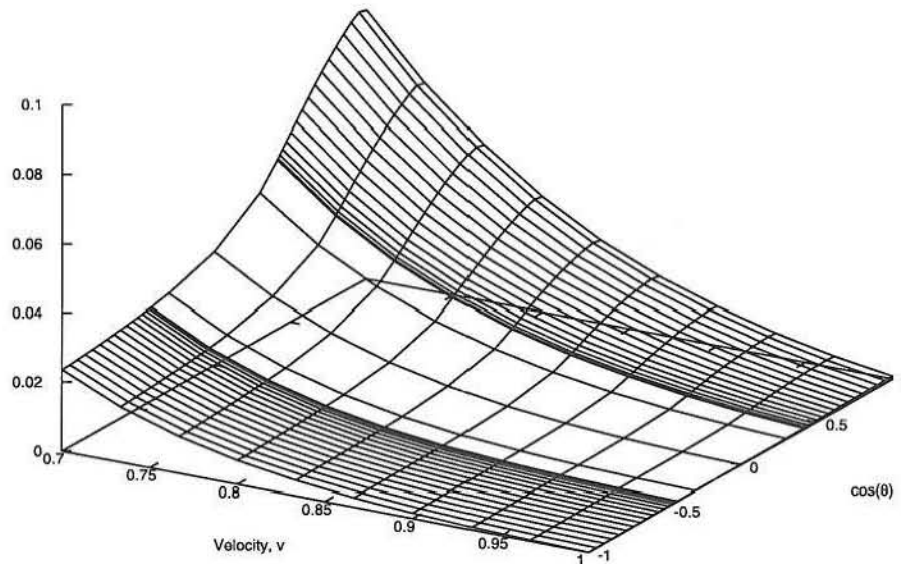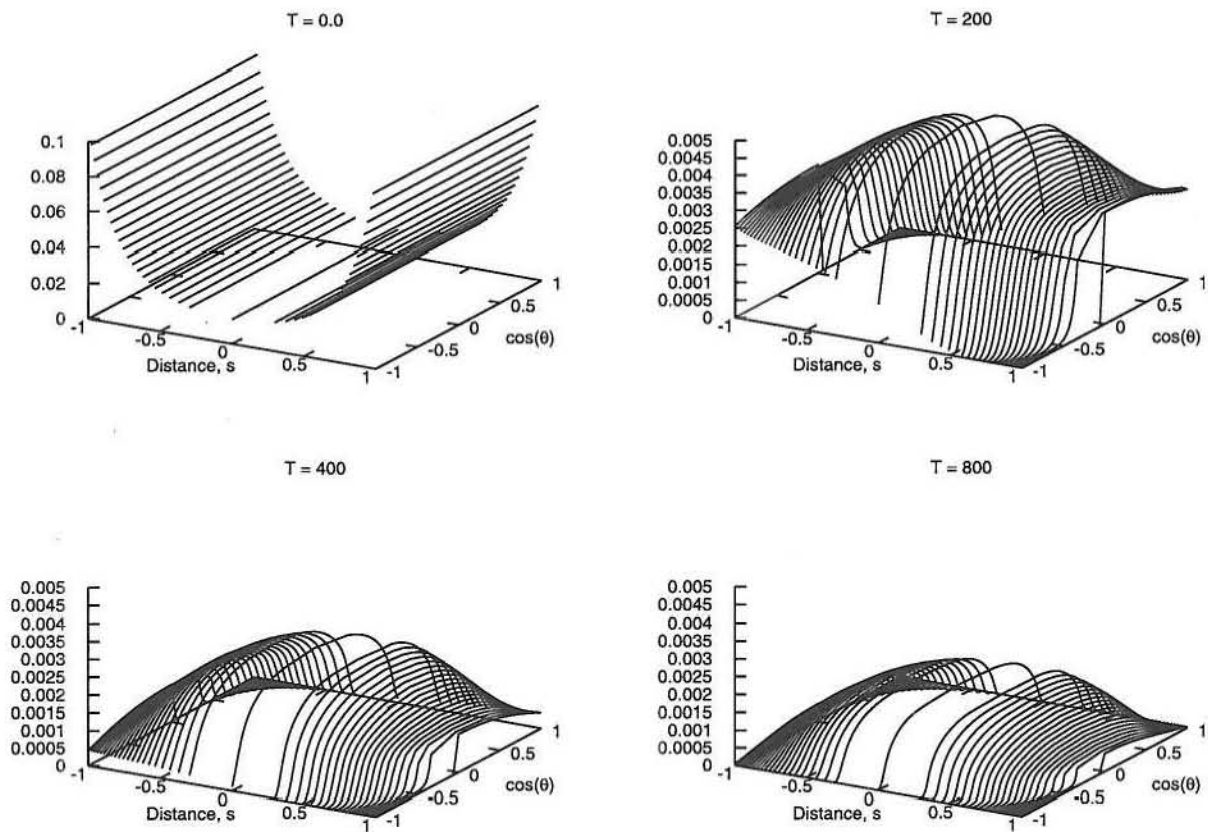Distribution at s=-0.96, T = 244   Distribution at s=-0.96, T = 400

Figure 12. Relaxation of the initial Maxwellian distribution function to stationary distribution at $s = -0.96$ as function of velocity v and the cosine of the pitch angle $\xi = \cos\theta$.
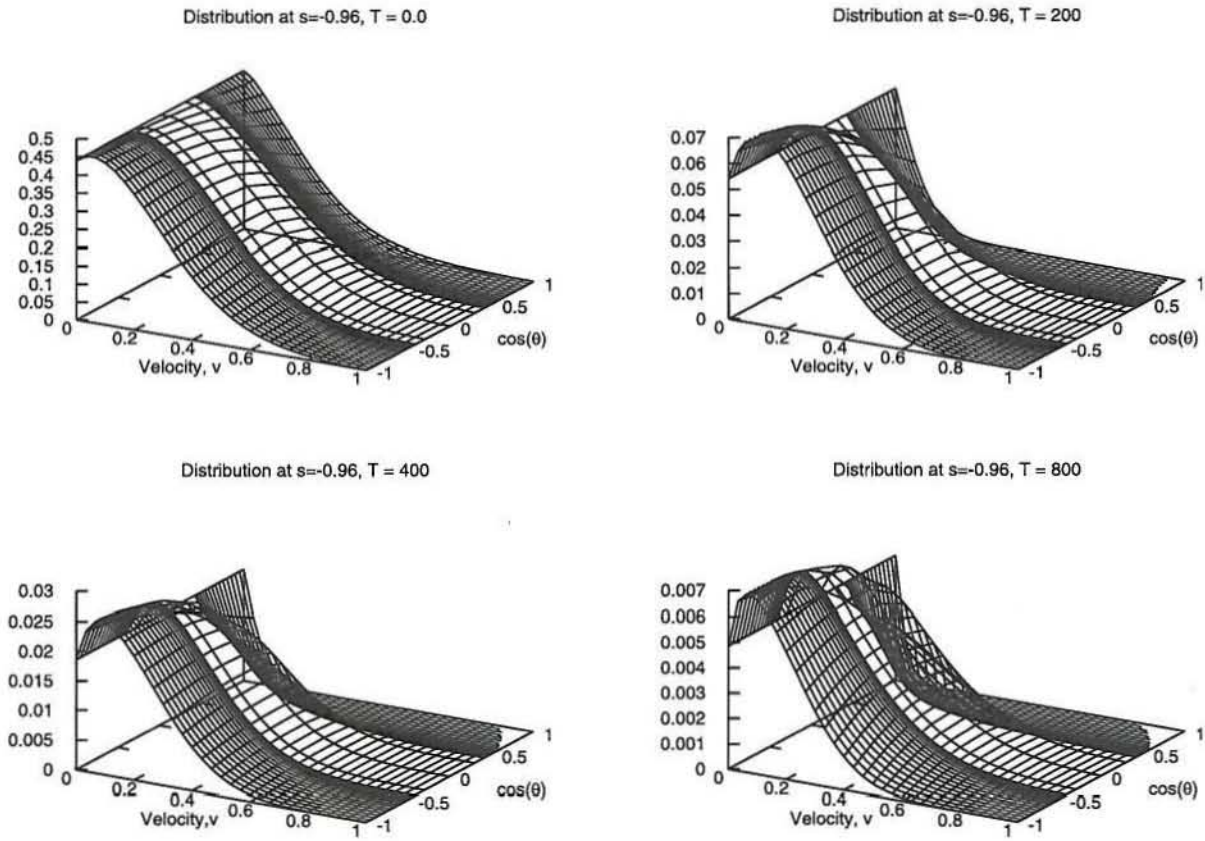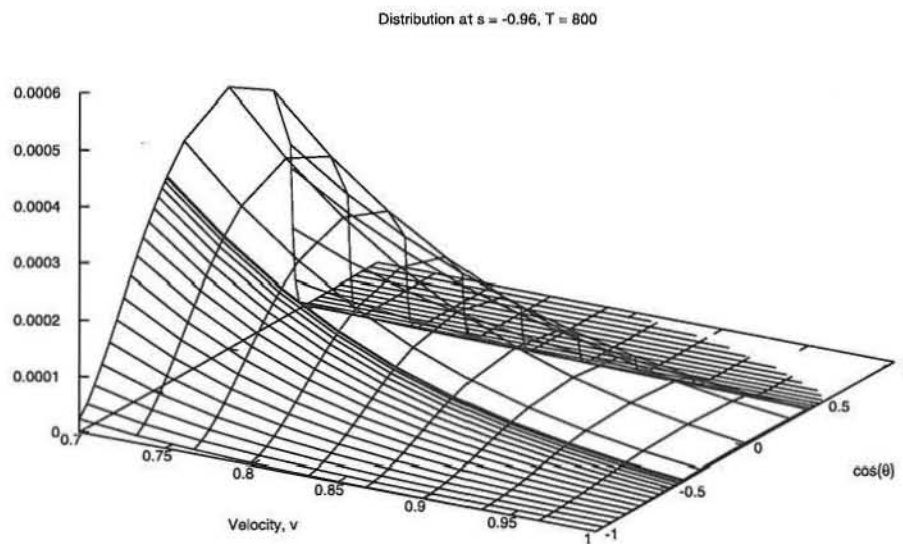
Distribution at s = -0.96, T = 400

Figure 13. High-energy part of the stationary distribution at $s = 0.96$ as function of velocity v and cosine of pitch angle $\xi = \cos\theta$.

Figure 14. Precipitation from the plasmaspheric tube with $L = 2$: distribution function at $v = 0.67$ as a function of distance s and cosine of pitch angle $\xi = \cos\theta$.

Distribution at s=-0.96, T = 0.0

Distribution at s=-0.96, T = 200

Distribution at s=-0.96, T = 400

Distribution at s=-0.96, T = 800

Figure 15. Precipitation from the plasmaspheric tube with $L = 2$: distribution function at $s = -0.96$ as a function of velocity v and cosine of pitch angle $\xi = \cos\theta$.

Distribution at s = -0.96, T = 800

Figure 16. Precipitation from the plasmaspheric tube with $L = 2$: high-energy portion of the distribution function at $s = -0.96$ as a function of velocity v and cosine of the pitch angle $\xi = \cos\theta$.

distribution function is very strong due to the very slow collision rate of high-energy particles.

6. Conclusions

[40] The kinetic Fokker-Planck model with an exact non-linear Coulomb collisional operator has been implemented numerically and tested. The concept of integration along the particle trajectories and time splitting technique has been developed and used. This allows us to obtain an accurate description of collisional relaxation of the particles in the presence of fast convection along the field lines in the loss cone, rapid circulation inside the trapped region, and relatively slower collisional diffusion of velocity space. The numerical model has been used to describe the plasma dynamics and transport in the plasmasphere between the conjugate regions of the ionosphere. The numerical modeling results have been presented in the form of time-dependent distribution functions of the charged particles along the geomagnetic dipole magnetic field line as a function of velocity and pitch angle. Results for high-energy tails of the distribution are compatible with the previous models, based on a simplified description of the Coulomb collisions.

[41] The use of exact form of Coulomb collisional operator allows us to overcome most serious limitations of the linearization procedure used in previous research. As a result, a complete picture of particle distribution function is available. This represents a major step toward the accurate self-consistent global modeling of the ionospheric outflows with inclusion of self-consistent electromagnetic effects and multiple plasma components.

References

Barakat, A. R., and J. Lemaire (1990), Monte Carlo study of the escape of a minor species, *Phys. Rev. A*, 42, 3291.

Barakat, A. R., and R. W. Schunk (1982a), Comparison of Maxwellian and bi-Maxwellian expansions with Monte Carlo simulations for anisotropic plasmas, *J. Phys. D*, 15, 2189.

Barakat, A. R., and R. W. Schunk (1982b), Comparison of transport equations based on Maxwellian and bi-Maxwellian distributions for anisotropic plasmas, *J. Phys. D*, 15, 1195.

Barakat, A. R., and R. W. Schunk (2001), Effects of wave-particle interactions on the dynamic behavior of the generalized polar wind, *J. Atmos. Sol. Terr. Phys.*, 63, 75, doi:10.1016/S1364-6826(00)00106-1.

Barakat, A. R., and R. W. Schunk (2006), A three-dimensional model of the generalized polar wind, *J. Geophys. Res.*, 111, A12314, doi:10.1029/2006JA011662.

Barakat, A. R., R. W. Schunk, and I. A. Barghouthi (1993), Monte Carlo study of the transition region in the polar wind: An improved collision model, *J. Geophys. Res.*, 98, 17,583.

Barakat, A. R., I. A. Barghouthi, and R. W. Schunk (1995), Double-hump h + velocity distribution in the polar wind, *Geophys. Res. Lett.*, 22, 1857.

Barakat, A., H. Thiemann, and R. Schunk (1998), Comparison of macroscopic particle-in-cell and semikinetic models of the polar wind, *J. Geophys. Res.*, 103, 29,277.

Barghouthi, I. A., A. R. Barakat, and R. W. Schunk (1993), Monte Carlo study of transition in the polar wind: An improved collision model, *J. Geophys. Res.*, 98, 17,583.

Barghouthi, I. A., S. H. Ghithan, and H. Nilsson (2011), A comparison study between observations and simulation results of Barghouthi model for O^+ and H^+ outflows in the polar wind, *Ann. Geophys.*, 29(11), 2061, doi:10.5194/angeo-29-2061-2011.

Demars, H. G., and R. W. Schunk (1989), Solutions to bi-Maxwellian transport equations for the polar wind, *Planet. Space Sci.*, 37, 85.

Demars, H. G., and R. W. Schunk (1994), A multi-ion generalized transport model of the polar wind, *J. Geophys. Res.*, 99, 2215.

Demars, H. G., and R. W. Schunk (1992), Semi-kinetic and transport models of the polar and solar winds, *J. Geophys. Res.*, 97, 1581.

Echim, M. M., J. Lemaire, and Ø. Lie-Svendsen (2011), A review on solar wind modeling: Kinetic and fluid aspects, *Surv. Geophys.*, 32, 1, doi:10.1007/s10712-010-9106-y.

Ganguli, S. B. (1996), The polar wind, *Rev. Geophys.*, 34, 311.

Ganguli, S. B., and H. G. Mitchell Jr. (1987), Behavior of ionized plasma in the high latitude topside ionosphere: The polar wind, *Planet. Space Sci.*, 35, 703.

Ganguli, S. B., H. G. Mitchell, and P. J. Palmadesso (1993), Plasma dynamics driven by finite-width current filament and kV potential drops in IM coupling, *Geophys. Res. Lett.*, 20, 975.

Gardner, L. C., and R. W. Schunk (2004), Neutral polar wind, *J. Geophys. Res.*, 109, A05301, doi:10.1029/2003JA010291.

Glocer, A., G. Tóth, T. Gombosi, and D. Welling (2009), Modeling ionospheric outflows and their impact on the magnetosphere: Initial results, *J. Geophys. Res.*, 114, A05216, doi:10.1029/2009JA014053.

Gombosi, T. I., and T. L. Killeen (1987), Effects of thermospheric motions on the polar wind: A time-dependent numerical study, *J. Geophys. Res.*, 92, 4725.

Gombosi, T. I., T. E. Cravens, and A. F. Nagy (1985), A time-dependent theoretical model of the polar wind: Preliminary results, *Geophys. Res. Lett.*, 12, 167.

Horwitz, J. L., and W. Zeng (2009), Physics-based formula representations of high-latitude ionospheric outflows: H^+ and O^+ densities, flow velocities, and temperatures versus soft electron precipitation, wave-driven transverse heating, and solar zenith angle effects, *J. Geophys. Res.*, 114, A01308, doi:10.1029/2008JA013595.

Khabibrakhmanov, I. K., and G. V. Khazanov (2000), The spectral collocation method for the kinetic equation with the nonlinear two-dimensional Coulomb collisional operator, *J. Comput. Phys.*, 161(2), 558.

Khazanov, G. V. (1979), *The Kinetics of the Electron Plasma Component of the Upper Atmosphere* [in Russian], Nauka, Moscow. [English translation, Natl. Transl. Cent., Washington, D. C., 1980.]

Khazanov, G. V., and M. W. Liemohn (1995), Nonsteady state ionosphere-plasmasphere coupling of superthermal electrons, *J. Geophys. Res.*, 100, 9669.

Khazanov, G. V., M. A. Koen, and G. S. Kudryashev (1978), The kinetics of electrons at the heights of 100–260 km [in Russian], *Radiophysica*, 21, 646.

Khazanov, G. V., M. A. Koen, and S. I. Burenkov (1979), A numerical solution to the kinetic equation for photoelectrons taking into account the free and trapped zones, *Cosmic Res.*, 17, 741.

Khazanov, G. V., M. A. Koen, Y. V. Konikov, and I. M. Sidorov (1984), Simulation of ionosphere-plasmasphere coupling taking into account ion inertia and temperature anisotropy, *Planet. Space Sci.*, 32, 585.

Khazanov, G. V., M. W. Liemohn, T. I. Gombosi, and A. F. Nagy (1993), Non-steady-state transport of superthermal electrons in the plasmasphere, *Geophys. Res. Lett.*, 20, 2821.

Khazanov, G. V., T. Neubert, and G. D. Gefan (1994), Kinetic theory of ionosphere-plasmasphere transport of suprathermal electrons, *IEEE Trans. Plasma Sci.*, 22, 187.

Khazanov, G. V., T. E. Moore, M. W. Liemohn, V. K. Jordanova, and M.-C. Fok (1996), Global, collisional model of high-energy photoelectrons, *Geophys. Res. Lett.*, 23, 331.

Khazanov, G. V., M. W. Liemohn, and T. E. Moore (1997), Photoelectron effects on the self-consistent potential in the collisionless polar wind, *J. Geophys. Res.*, 102, 7509.

Killeen, J., A. A. Mirin, and M. E. Rensink (1976), The solution of the kinetic equations for a multispecies plasma, in *Controlled Fusion, Methods Comput. Phys.*, vol. 16, pp. 389–431, Academic, New York.

Körösmezey, A., C. E. Rasmussen, T. I. Gombosi, and G. V. Khazanov (1992), Anisotropic ion heating and parallel O^+ acceleration in regions of rapid $E \times B$ convection, *Geophys. Res. Lett.*, 19, 2289, doi:10.1029/92GL02489.

Lemaire, J., and M. Scherer (1972), Ion-exosphere with asymmetric velocity distribution, *Phys. Fluids*, 15, 760.

Lie-Svendsen, Ø., and M. H. Rees (1996), An improved kinetic model for the polar outflow of a minor ion, *J. Geophys. Res.*, 101, 2415.

Marchuk, G. I. (1975), *Methods of Numerical Mathematics*, *Appl. Math.*, vol. 2, Springer, New York.

Miller, R. H., and M. R. Combi (1994), A coulomb collision algorithm for weighted particle simulations, *Geophys. Res. Lett.*, 21, 1735.

Miller, R. H., T. I. Gombosi, C. E. Rasmussen, G. V. Khazanov, and D. Winske (1993), A kinetic simulation of plasma flows in the inner magnetosphere, *J. Geophys. Res.*, *98*, 19,301.

Miller, R. H., C. E. Rasmussen, M. R. Combi, T. I. Gombosi, and D. Winske (1995), Ponderomotive acceleration in the auroral region: A kinetic simulation, *J. Geophys. Res.*, *100*, 23,901.

Mitchell, H. G., Jr., and P. J. Palmadesso (1983), A dynamic model for the auroral field line plasma in the presence of field-aligned current, *J. Geophys. Res.*, *88*, 2131.

Moffett, R. J., G. J. Bailey, S. Quegan, Y. Rippeth, A. M. Samson, and R. Seller (1989), Modelling the ionospheric and plasmaspheric plasma, *Philos. Trans. R. Soc. A, 328*, 255.

Pierrard, V., and J. Lemaire (1998), A collisional kinetic model of the polar wind, *J. Geophys. Res.*, *103*, 11,701, doi:10.1029/98JA00628.

Pierrard, V., M. Maksimovic, and J. Lemaire (2001), Self-consistent model of solar wind electrons, *J. Geophys. Res.*, *106*, 29,305, doi:10.1029/2001JA900133.

Rasmussen, C. E., and R. W. Schunk (1988), Multistream hydrodynamic modeling of interhemispheric plasma flow, *J. Geophys. Res.*, *93*, 14.

Rosenbluth, M. N., W. M. MacDonald, and D. L. Judd (1957), Fokker-Planck equation for an inverse-square force, *Phys. Rev.*, *107*, 1.

Schunk, R. W. (1986), An updated theory of the polar wind, *Adv. Space Res.*, *6*(3), 79.

Schunk, R. W. (1988a), Polar wind tutorial, in *Physics of Space Plasmas*, edited by T. Chang, G. B. Crew, and J. R. Jasperse, p. 81, Scientific, Cambridge, Mass.

Schunk, R. W. (1988b), The polar wind, in *Modeling Magnetospheric Plasma*, *Geophys. Monogr. Ser.*, vol. 44, edited by T. E. Moore and J. H. Waite, p. 219, AGU, Washington, D. C.

Schunk, R. W., and J. J. Sojka (1989), A three-dimensional time-dependent model of the polar wind, *J. Geophys. Res.*, *94*, 8973.

Schunk, R. W., and D. S. Watkins (1979), Comparison of solutions to the thirteen moment and standard transport equations for low speed thermal proton flows, *Planet. Space Sci.*, *27*, 433.

Shkarofsky, I. P., T. Johnston, and M. P. Bachynsky (1966), *The Particle Kinetics of Plasmas*, Addison-Wesley, London.

Singh, N., and J. L. Horwitz (1992), Plasmaspheric refilling, *J. Geophys. Res.*, *97*, 1049.

Singh, N., and R. W. Schunk (1985), Temporal behavior of density perturbations in the polar wind, *J. Geophys. Res.*, *90*, 6487.

Singh, N., and D. G. Torr (1990), Effects of ion temperature anisotropy on the interhemispheric plasma transport during plasmasperic refilling, *Geophys. Res. Lett.*, *17*, 925.

Tam, S., F. Yasseen, T. Chang, and S. B. Ganguli (1995), Self-consistent kinetic photoelectron effects on the polar wind, *Geophys. Res. Lett.*, *22*, 2107.

Wilson, G. R. (1992), Semikinetic modeling of the outflow of ionospheric plasma through the topside collisional to collisionless region, *J. Geophys. Res.*, *97*, 10.

Wilson, G. R., C. W. Ho, J. L. Horwitz, N. Singh, and T. E. Moore (1990), A new kinetic model for time-dependent polar plasma outflow: Initial results, *Geophys. Res. Lett.*, *17*, 263.

Yau, A., T. Abe, and W. Peterson (2007), The polar wind: Recent observations, *J. Atmos. Sol. Terr. Phys.*, *69*(16), 1936, doi:10.1016/j.jastp.2007.08.010.

Yasseen, F., J. M. Retterer, T. Chang, and J. D. Winningham (1989), Monte-Carlo modeling of polar wind photoelectron distributions with anomalous heat flux, *Geophys. Res. Lett.*, *16*, 1023.